Accuracy of the classical trajectory Monte Carlo method for electron capture in Li^{3+} and $Ne^{10+}+H(1s)$ collisions

L. F. Errea,[1] Clara Illescas,[1] L. Méndez,[1] B. Pons,[2] A. Riera,[1] and J. Suárez[1,*]

[1]*Laboratorio Asociado al CIEMAT de Física Atómica y Molecular en Plasmas de Fusión, Departamento de Química C-IX, Universidad Autónoma, 28049 Madrid, Spain*

[2]*Centre Lasers Intenses et Applications, UMR 5107 du CNRS, Université de Bordeaux–I, 351 Cours de la Libération, 33405 Talence, France*

(Received 10 June 2004; published 24 November 2004)

The accuracy of classical trajectory Monte Carlo treatments of electron capture is studied, by focusing on collisions on H(1*s*) targets by Li^{3+} and Ne^{10+} projectiles, treated in a separate paper. We examine how the choice of the initial distribution, and the partition of phase space usually employed to calculate partial cross sections, influence the accuracy of the method. With respect to the former, an improvement over the single-microcanonical choice is advisable, but further refinements based on the electron density are not worthwhile. Regarding the latter, we illustrate the accuracy of the "binning" method for $n>2$. We show that classical and semiclassical mechanisms are essentially the same, although at low velocities the method is unable to describe the fall of the cross section.

DOI: 10.1103/PhysRevA.70.052713 PACS number(s): 34.10.+x, 34.70.+e

I. INTRODUCTION

Despite the large amount of research carried out on the subject, the conditions of validity of the computational techniques of classical physics remain an open question, whose answer depends not only on the nature of the problem but also on the particular method employed. This is because few of these methods are purely classical, and most of them incorporate quantal effects in some form or another. Such is the case, in the field of atomic collisions, of the classical trajectory Monte Carlo (CTMC) method, originally developed by Abrines and Percival [1], and whose basis has been examined in, e.g., Refs. [2–4]. Its success is due to both its ease of application and its accuracy. With respect to the former, the simplicity of its algorithms stand in sharp contrast with, say, close-coupling programs that require additionally a considerable amount of "know-how." Regarding the accuracy, the CTMC method has been successfully employed to obtain reliable total (see, e.g., [5–9]) and partial capture (e.g., [10–12]) cross sections, using either the so-called three-body [5] or the impact-parameter [13] version. Moreover, the method works best in the (difficult) energy domain where ionization and electron capture compete with each other, and its precision is not limited to the cross sections, extending [14] to the ionization probabilities and even spatial and momentum densities, when an accurate initial distribution is employed [15]. In addition, it can provide pictorial tools for the description of the mechanisms [14,16–18].

Since publications usually report positive results, it is useful for potential users to know the limits within which successful methods can be safely employed. In this spirit, an analysis of the limitations of close-coupling methods has been presented in Ref. [19] for molecular expansions and in Ref. [20] for atomic bases. Likewise, a study of the accuracy of the CTMC method for ionization has been presented in Refs. [14,20]. However, such a study is lacking for electron capture, even though some features are worth investigating.

A well known limitation at low v concerns the inability of the classical approach to treat $H^+ + H$ resonant charge exchange, for obvious reasons. However, in the other extreme of highly charged projectile impact on H, very little is known of the accuracy of the method. The answer is useful, because the computational effort of the CTMC approach is roughly independent of the nuclear charge, which is certainly not the case of close-coupling techniques; it would thus be very useful to treat, e.g., collisions of atomic hydrogen and helium targets with highly charged ions such as Ne^{10+} or Ar^{18+}, which have recently become of strong interest in the study of fusion plasmas. Another point to be elucidated is the accuracy of probabilities and partial cross sections. A third aspect is whether this accuracy has a physical basis, arising from a common mechanism with quantal approaches, or is partially coincidental, and what are the main features of the method that determine its limitations.

Regarding the first point of accuracy of the CTMC method, its success was confirmed by explicit calculations [8] for impact of H(1*s*) with ions ranging from H^+ to O^{8+}. This was further corroborated by a recent treatment ([21], hereafter called Paper I) for Ne^{10+} impact on H, in which calculated capture and ionization cross sections are accurate over a wide range of energies ($10 \leqslant E \leqslant 250$ keV amu^{-1}) as compared to converged close-coupling results using a very large basis. From all these data alone, one would tend to conclude that the accuracy of CTMC treatments improves with the nuclear charge of the projectile. However, it was also found in Paper I that the excellent accuracy does not quite extend to the partial cross sections, which led us to investigate the limits of confidence of the classical method, using the molecular calculations as a standard of comparison. In addition, since Paper I treated both $Li^{3+}+H$ and Ne^{10+}

*Author to whom correspondence should be addressed. Electronic address: jaime.suarez@uam.es

collisions, we were able to analyze the dependence of the main features on the charge of the projectile. We further extended the analysis to find out to what extent the limitation of the method depends on what are usually considered the optional aspects of the CTMC method. For the sake of cogency, our main findings on these topics are described separately in the present paper.

In the next section we briefly state some details of the methods that are additional to those given in Paper I. In Secs. III and IV we focus our attention on the delicate topic of the incorporation of quantal aspects in the asymptotic regions where reaction channels are defined. The accuracy of capture and ionization cross sections is discussed in Sec. V, and analyzed through the mechanisms in Sec. VI. Our main conclusions are drawn in Sec. VII.

Atomic units are employed except where otherwise stated.

II. SEMICLASSICAL AND CLASSICAL METHODS

In the semiclassical treatment of Paper I, we employed an impact-parameter formalism, in which the electronic wave function satisfies a time-dependent Schrödinger equation for the Born-Oppenheimer fixed-nuclei Hamiltonian $\hat{H}$, and the internuclear vector $\mathbf{R}=\mathbf{b}+\mathbf{v}t$ follows a linear trajectory with impact parameter $\mathbf{b}$ and velocity $\mathbf{v}$. To establish a connection with classical calculations, we introduce as in Ref. [14] the polar form of the wave function representing the electronic motion:

$$\Psi(\mathbf{r},t)=|\Psi(\mathbf{r},t)|e^{iS(\mathbf{r},t)}=\sqrt{\rho_Q(\mathbf{r},t)}e^{iS(\mathbf{r},t)}. \tag{1}$$

Substitution in the Schrödinger equation yields the continuity equation for the density:

$$\frac{\partial \rho_Q}{\partial t}=-\nabla\cdot\mathbf{j}_Q=-\nabla\cdot(\rho_Q\nabla S). \tag{2}$$

As explained in Paper I, to solve the impact parameter equation, we expanded Ψ in a close-coupling series in terms of a basis of the so-called one-electron-diatomic-molecule (OEDM) orbitals χ_j of the LiH^{3+} or NeH^{10+} quasimolecule, modified with a common translation factor (CTF) U [22–25]:

$$\Psi(\mathbf{r},v,b,t)=e^{iU(\mathbf{r},t)}\sum_k a_k(v,b,t)\chi_k(\mathbf{r},R)\exp\left(-i\int_0^t E_k(t')dt'\right). \tag{3}$$

The CTF is mainly introduced to satisfy the limit conditions of the problem, so that the basis functions $\chi_j\exp(iU)$ are uncoupled at infinite internuclear separations. As is well known, this requirement only determines the mathematical form (plane waves) of the electronic translation factors (ETF's) in this asymptotic limit. For finite internuclear distances R, the CTF approach chooses an R-dependent interpolative form between the plane waves corresponding to the projectile and to the target channels, which is defined in terms of a switching function $f(\mathbf{r},\mathbf{R})$:

$$U(\mathbf{r},t)=f(\mathbf{r},\mathbf{R})\mathbf{v}\cdot\mathbf{r}-\frac{1}{2}f^2(\mathbf{r},\mathbf{R})v^2t. \tag{4}$$

To extend the molecular expansion to high energies, where ionization starts to be sizable, we have carried out calculations by adding to the OEDM basis a set of Gaussian functions, centered on an intermediate point of the internuclear axis, and whose populations yield the ionization probability; this is the expansion called OEDM+GTO (Gaussian-type orbital). The basis set for $Li^{3+}+H(1s)$ collisions includes 35 OEDM orbitals and a set of 80 GTOs. For $Ne^{10+}+H(1s)$ we employed a set of 213 OEDMs. Details of these basis sets are given in Paper I.

As explained in Paper I, and in parallel with the semiclassical approach, our classical work employed an impact-parameter CTMC method, in which the internuclear vector follows linear trajectories, and the electronic probability distribution $\rho(\mathbf{r},\mathbf{p},t)$ is generated through an N-point discrete representation of this distribution:

$$\rho(\mathbf{r},\mathbf{p},t)=\frac{1}{N}\sum_{j=1}^{N}\delta(\mathbf{r}-\mathbf{r}_j(t))\,\delta(\mathbf{p}-\mathbf{p}_j(t)), \tag{5}$$

where $\mathbf{r}$ and $\mathbf{p}$ are the position and momentum vector of the electron, respectively, with respect to the target nucleus. Substitution of the pointwise representation in the Liouville equation then yields the Hamilton equations for the individual $\mathbf{r}_j(t),\mathbf{p}_j(t)$ trajectories. Initial conditions for these equations were obtained from a sampling of a statistical distribution $\rho(\mathbf{r},\mathbf{p})$ for the $H(1s)$ state, which was taken to be either a microcanonical distribution $\rho^m(\mathbf{r},\mathbf{p};E)$, or superpositions of such distributions; by substitution in the Liouville equation, both choices are seen to be time independent in the absence of the projectile. In our calculations, we considered continuum superpositions

$$\rho(\mathbf{r},\mathbf{p})=\int\rho_E(E)\rho^m(\mathbf{r},\mathbf{p};E)dE=2^{-1/2}\pi^{-3}\times\int(-E)^{5/2}\rho_E(E)\,\delta(H-E)dE \tag{6}$$

as well as discrete sums

$$\rho(\mathbf{r},\mathbf{p})=\sum_j w_j\rho^m(\mathbf{r},\mathbf{p};E_j)=2^{-1/2}\pi^{-3}\sum_j w_j(-E_j)^{5/2}\delta(H-E_j) \tag{7}$$

to be discussed in Sec. IV.

The Hamilton equations were integrated [26] up to internuclear distances of the order of 10^3 to achieve full convergence of the densities and probabilities. For each nuclear trajectory, the capture transition probabilities are given by the relative number of asymptotic trajectories that yield a negative energy with respect to the projectile and a positive energy with respect to the target; similarly, ionization probabilities are obtained from the relative number of asymptotic trajectories that have positive energies with respect to both nuclei. Total cross sections are then given by summing the corresponding probabilities over all nuclear trajectories. Par-

tial cross sections to a given n state were obtained by the usual partitioning of phase space into n,l "bins," due to Becker and MacKellar (hereafter called BM) [27]. A simple connection between the CTMC and the semiclassical approaches can formally be obtained by integrating Liouville's equation with respect to the momentum variables. This yields a continuity equation for the spatial density $\rho(\mathbf{r},t)$:

$$\frac{\partial \rho(\mathbf{r},t)}{\partial t} = -\nabla \cdot \mathbf{j} = -\nabla \cdot \int \mathbf{p}\ \rho(\mathbf{r},\mathbf{p},t)d\mathbf{p}, \tag{8}$$

which is analogous to Eq. (2). However, as pointed out in Ref. [14], it would be misleading to pursue the connection by employing in Eq. (2) the standard textbook WKB limit form of S, which is the classical characteristic function S_C. It was shown in that reference that for ionization the accuracy of the CTMC method is far superior to what one would expect from the WKB approach—which is rather poor since the wavelength corresponding to the ionized electron is of the size of the colliding region.

At first sight, a better connection between classical and quantal statistical approaches was pointed out in Ref. [4], in terms of quantal Wigner distributions (see Ref. [28]), and the Moyal-Wigner equation (Ref. [29]) whose classical limit in natural units ($\hbar \to 0$) is the Liouville equation. However, unlike this latter equation, the Moyal-Wigner counterpart, even when truncated to $O(\hbar^2)$, does not seem to be amenable to a discretization procedure leading to electron trajectories, so that one is compelled to work within the classical limit. This, however, has the inconvenience that the Wigner function is unstable when its evolution is treated in this classical limit, and also has some unphysical properties when considered in a classical context [30] (see Sec. IV). Hence, though formally appealing, this line of thought has not been actually pursued in a quantitative way.

A less formalistic approach to the connection between classical and quantal methods was taken in Ref. [14] for ionization, and we briefly recall the arguments. To start with, for any reasonable initial distribution, $\mathbf{j}=\mathbf{0}=\mathbf{j}_Q$. Furthermore, as shown in Ref. [20], the asymptotic form for the ionized current also satisfies $\mathbf{j} \approx \rho \mathbf{r}/t \approx \rho_Q \nabla S_Q = \mathbf{j}_Q$ for sufficiently large r (and t) values. The accuracy of the CTMC method was then reasoned to follow from these two asymptotic relations for the current, together with a good description of electron-projectile collisions in the intermediate region, where ionization is dominated by a direct mechanism yielding soft electrons. In turn, such a description is understandable from the well-known fact that the two-body Rutherford differential cross sections in classical and quantum mechanics coincide (for a recent comparison of classical and quantum mechanical Rutherford scattering, see, e.g., Ref. [31]).

We now apply a similar reasoning to electron capture. We again consider three regions: (i) the initial stage of the collision, where $\rho \approx \rho_Q$ and $\mathbf{j}=\mathbf{j}_Q=\mathbf{0}$; (ii) the intermediate stage, where a departure of the CTMC density from its quantal analog is expected only when three-body effects are sizable; and (iii) the exit asymptotic region, where the capture part of the distribution $\rho_{\rm cap}(\mathbf{r},\mathbf{p},t)$ peaks about $\mathbf{p}=\mathbf{v}$, so that, using a peaking approximation,

$$\mathbf{j}_{\rm cap} = \int \mathbf{p}\ \rho_{\rm cap}(\mathbf{r},\mathbf{p},t)d\mathbf{p} \approx \mathbf{v}\int \rho_{\rm cap}(\mathbf{r},\mathbf{p},t)d\mathbf{p} \equiv \mathbf{v}\rho_{\rm cap}(\mathbf{r},t)$$
$$\approx \mathbf{v}\rho_{Q\rm cap}(\mathbf{r},t). \tag{9}$$

Now, since for the capture component in the close-coupling expansion, the $\mathbf{r}$ dependence of its phase S in this asymptotic region takes essentially the form of the ETF, we have that $\mathbf{j}_{Q\rm cap}=\rho_{Q\rm cap}\nabla S_{\rm cap} \approx \mathbf{v}\rho_{Q\rm cap}$ too. This ensures that the total capture cross sections are close to each other. The accuracy of partial cross sections then depends on how this capture distribution $\rho_{\rm cap}(\mathbf{r},\mathbf{p},t)$ is partitioned into (nl) subsets, which brings up the question of how well are the final states represented by the method of BM. Since the first subset corresponds to the initial state, which must also be described reasonably well [step (i) above], we see that points (i) and (ii) are related, and we start our analysis on how quantal effects are introduced in the CTMC method by the partition method.

III. ACCURACY OF FINAL STATES

In the asymptotic $t \to \infty$ domain, each trajectory $\mathbf{r}_j(t),\mathbf{p}_j(t)$ describing a captured electron has a definite, constant energy E_{pj} with respect to the projectile, and may therefore be considered as yielding a pointwise contribution $\rho^m(\mathbf{r}_j,\mathbf{p}_j,E_{pj})\delta(\mathbf{p}-\mathbf{p}_j(t))\delta(\mathbf{r}-\mathbf{r}_j(t))$ to the statistical distribution. Adding up all trajectories, we obtain a sampling that may be considered as a discretized approximation to a continuous superposition of the same form of Eq. (6):

$$\rho_{\rm cap}(\mathbf{r},\mathbf{p}) = N_{\rm cap}^{-1}\sum_j^{N_{\rm cap}} \delta(\mathbf{p}-\mathbf{p}_j(t))\,\delta(\mathbf{r}-\mathbf{r}_j(t))\rho^m(\mathbf{r}_j,\mathbf{p}_j;E_{pj})$$
$$\approx \int \rho_E(E_p)\rho^m(\mathbf{r},\mathbf{p};E_p)dE_p, \tag{10}$$

where now $\rho_E(E_p)$ is a *final* density of projectile states.

As explained in paper I, the BM method ascribes each trajectory of a captured electron to an atomic quantum state by means of a partitioning of the phase space into subsets or "bins" [7,27,32], and the ratio of trajectories falling into each subset to the total number of trajectories then gives the corresponding partial probability. For the principal quantum number n the bins are defined by $c^{(n)} \leqslant n_c Z_p/\sqrt{-2E_p} < c^{(n+1)}$, or equivalently by $E^{(n)} \leqslant E_p < E^{(n+1)}$ with $E^{(n)}=-Z_p^2/2(c^{(n)})^2$ and $n_c=\sqrt{-1/2E}$. The values of $c^{(n)}$ are obtained from the condition that the volume of phase space divided by $(2\pi)^3$ (in a.u.) equals the multiplicity n^2 of the n shell. This condition is obviously based on the high-n correspondence principle, and yields [33]

$$(c^{(n+1)})^3 - (c^{(n)})^3 = 3n^2. \tag{11}$$

The solution of this set of difference equations with the initial bin starting at $c^{(1)}=0$ is

$$(c^{(n)})^3 = (n-1/2)(n-1)n. \tag{12}$$

A similar "binning" $l/n < L/n_c \leqslant (l+1)/n$ [7,27] (see also Ref. [33]) employed for the l quantum number and the exit classical angular momentum L yields an (n,l) partial distri-

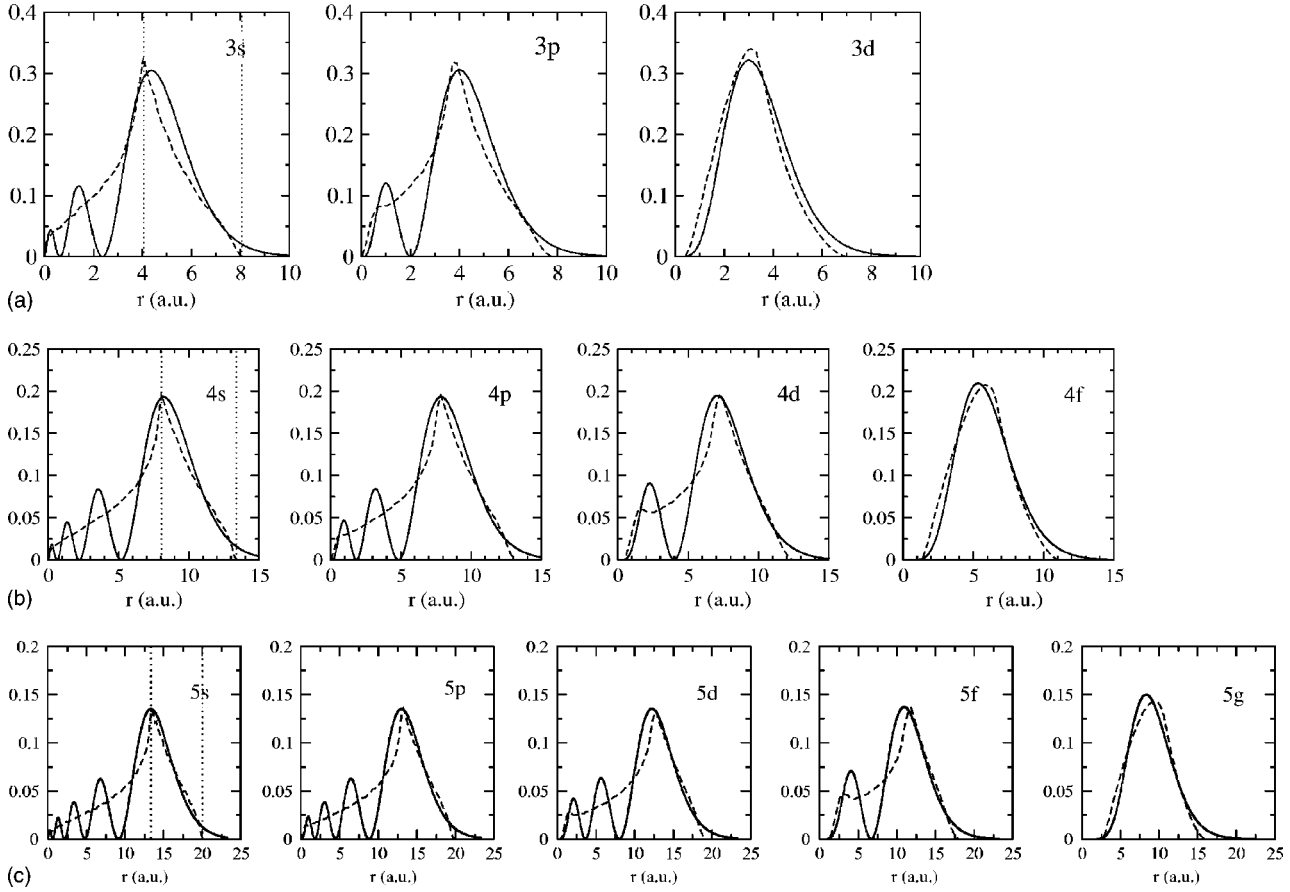

FIG. 1. Radial density function for different *nl* levels in Li: —, quantum; - - -, obtained from binning [27].

bution that may be considered as a discretized approximation to

$$\rho_{(nl)}(\mathbf{r},\mathbf{p}) = \int_{E^{(n)}}^{E^{(n+1)}} \rho_E(E_p)\rho^m(\mathbf{r},\mathbf{p};E_p,l)dE_p, \qquad (13)$$

and this yields the corresponding partial transition probability

$$P_{nl}(v,b) = \int d\mathbf{r} \int d\mathbf{p}\ \rho_{nl}(\mathbf{r},\mathbf{p}) \qquad (14)$$

and cross section

$$\sigma_{nl}(v) = 2\pi \int db\ P_{nl}(v,b). \qquad (15)$$

Since the procedure depends on the partition method employed, a pertinent question is whether the final (spatial and momentum) densities actually obtained in collisions bear a relation to the exact quantal ones, which is an aspect that does not appear to have been explicitly checked. Upon inspection, we have found that for $n>2$ densities are indeed reasonably accurate for the collisions considered here. We now display an illustration of this point which is independent of any particular impact parameter or nuclear velocity. Starting from Eq. (10) for the case of a projectile Li^{3+}, we can reason that for high n values the energy interval $E^{(n)} \leqslant E_p < E^{(n+1)}$ is so small so that one can take an average value $\rho_E(E_p) \approx ct$ within this interval, yielding an approximation which, once normalized to unity, takes the form

$$(E^{(n)} - E^{(n+1)})^{-1} \int_{E^{(n)}}^{E^{(n+1)}} \rho^m(\mathbf{r},\mathbf{p};E_p,l)dE_p. \qquad (16)$$

This approximation to the distribution of the *nl* state can then be employed to obtain the corresponding spatial radial density and compare it to the quantal counterpart $4\pi r^2|\chi(\mathbf{r})|^2$. We display these comparisons in Fig. 1 for $n=3$, 4, 5. As expected, the classical densities exhibit no nodes; furthermore, the *s* component peaks at $r=Z_p/E^{(n)}$, and all components vanish at $r=Z_p/E^{(n+1)}$, both features resulting from the binning procedure and the discontinuous character of the microcanonical radial density $\rho^m(\mathbf{r},E)$ [hence of the integrand in (10)], which abruptly vanishes for $r>Z/E$. On the whole, the overall comparison between classical and exact densities is rather good, and improves with increasing *l*. Although our illustrations employ an averaging approximation, we stress that the densities actually obtained in our collisional calculations exhibit the same shapes and behavior. We thus conclude that the BM procedure provides a physically sound procedure for the most important, outer part of the atomic orbitals for $n>2$.

For $n=2$ the results (not shown) are less good but still reasonable. This is not so for the 1*s* state, for which a direct comparison of the collisional densities (the previous uniform

approximation is obviously meaningless in this case) shows that the results are quite inaccurate. This is is not surprising, in view of the use of the correspondence principle to obtain the partition method, and is of little importance in the present applications, since capture to $Li^{2+}(1s)$ or $Ne^{9+}(1s)$ is negligible. A more detailed study shows that the results of the partition method are most sensitive to the boundary between the $n=1$ and 2 subsets. Another, more important, consequence is that the procedure cannot be employed to construct the initial H(1*s*) state of the system, so that one is obliged to employ different methods in the initial and exit regions to relate the corresponding classical and quantal densities. This gives the CTMC approach what seems to be an unavoidable "asymmetrical" character.

IV. ACCURACY OF INITIAL 1*s* STATE

Following the original proposal of Ref. [1], most CTMC calculations for ion impact on H(1*s*) have employed as initial condition a microcanonical phase space distribution for the target, $\rho^m(\mathbf{r},\mathbf{p},-0.5\ \text{a.u.})$. This is known to yield a momentum density that is identical to the quantal one, but a spatial density that is too compact, with a cutoff value at $r=2$ a.u. If one wishes to offset this liability, one can relax the restriction of a sharp classical energy value. One possibility, suggested by Eichenauer and Scheid [30] is to employ the Wigner function, so that both spatial and momentum densities are exact. However, the Wigner function, considered as a classical distribution, is unstable in time, among other undesirable features such as yielding a sizable number of electrons with positive energies, so that, even in the absence of a projectile and for all impact parameters and nuclear velocities, it would yield a nonzero ionization probability. This shows the dangers of a classical interpretation of the Wigner function, even where it is definite positive.

To preserve stability in time in the absence of the projectile, one can employ superpositions of microcanonical distributions with different energy values, as in Eq. (6) or (7). For instance, Hardie and Olson [15] employed a sum of eight microcanonical distributions (7) with energies E_j falling within the BM bin for the initial state (so as to avoid artificial excitation in the absence of the projectile) and chosen from equidistant cutoff values $-1/E_j$ of the corresponding densities $\rho^m(\mathbf{r},E_j)$; the corresponding weights w_j in Eq. (7) were chosen from a least-squares fit of the quantal density. It was further checked that a reasonable momentum density was also obtained. Results were then seen to be better than the single-microcanonical ones (see, e.g., Ref. [8]).

The finite sum method has the inconvenience that the derivative of the initial radial density is discontinuous. This is avoided by employing a continuous superposition such as Eq. (6), which is a function $\rho(\mathbf{r},\mathbf{p})=f(H)$ of H alone, and which also yields a stable distribution. In the work of Cohen [34], f was chosen such that the spatial density is exact, and the corresponding momentum density was checked to be reasonably accurate. This procedure appears to be marred by the complicated form of $f(H)$ and from the fact that a small tail of $\rho_E(E)$ falls outside the BM 1*s* bin, besides some unimportant odd features such as a negative energy density at very low energies. In a further contribution, Raković *et al.* [33] reasoned that neither spatial nor momentum densities should be preferred, and proposed a simpler Gaussian form for $f(H)$, with a dispersion parameter that is obtained by optimizing a combined fit of spatial, momentum, and intermediate densities.

In Fig. 2 we display a comparison of the radial spatial and momentum densities, respectively, obtained with the previous methods. We have also included the densities obtained with two additional procedures: (i) that of improving the fit of the spatial density given in Ref. [15], by using a sum of ten microcanonical distributions in Eq. (7), and (ii) that of employing in Eq. (6) an energy density $\rho_E(E)$ that takes a Gaussian form in terms of a classical analog of the n quantum number, $n_c=\sqrt{-1/2E}$, with a cutoff for $n_c<0.5$ a.u., and whose dispersion parameter is determined by the condition that the mean energy $\langle E\rangle=-0.5$ a.u. The main characteristics of the distributions considered are given in Tables I (discrete forms) and II (continuous forms). In our calculations, we substituted in Eq. (6) the continuous distributions by extremely fine grids of discrete representations.

In Fig. 2 we show that, in spite of their rather different generating conditions, both Gaussian forms yield very close results, and that all forms provide good approximations to spatial and momentum densities. The discrete forms (7) are aesthetically less appealing, and, from the practical side, the effect of their discontinuities in the derivatives is not obvious. However, they have the property that the corresponding energies all fit within the 1*s* bin, whereas the continuous superpositions involve energies $E>-0.24$ a.u., which, according to the binning procedure, would really describe excited states H(2*s*). The question whether this is a liability for capture and ionization can only be answered by explicit calculations.

V. COMPARISON OF CROSS SECTIONS

In the previous sections we have seen that the partitioning method is a simple, and for $n>2$ a reasonably accurate, procedure to impose quantal conditions in the exit stage of the collisional process; furthermore, it is a method that is not easily improved. On the other hand, for the initial state we have several possibilities, and it is worth finding out whether the results are actually affected by these different choices.

We first consider $Li^{3+}+H$ collisions. We display in Fig. 3 the total capture (a) and ionization (b) cross sections obtained using the CTMC method described in Sec. II, together with experimental [35–37] and accurate theoretical [5,38–45] data. Although the comparison with these data is discussed in Paper I, they are also included here as a guide to the eye regarding the accuracy of the different classical results.

We first comment here that Fig. 3(a) is quite typical of what we expect of the CTMC method for capture by a lowly charged ion. We note that the scale has been chosen so as to highlight the failure of the classical method to describe electron capture at low nuclear velocities. Results in the higher-energy range ($v>1.2$ a.u.) and for ionization are reasonably accurate, as reported in paper I. Our next comment is that

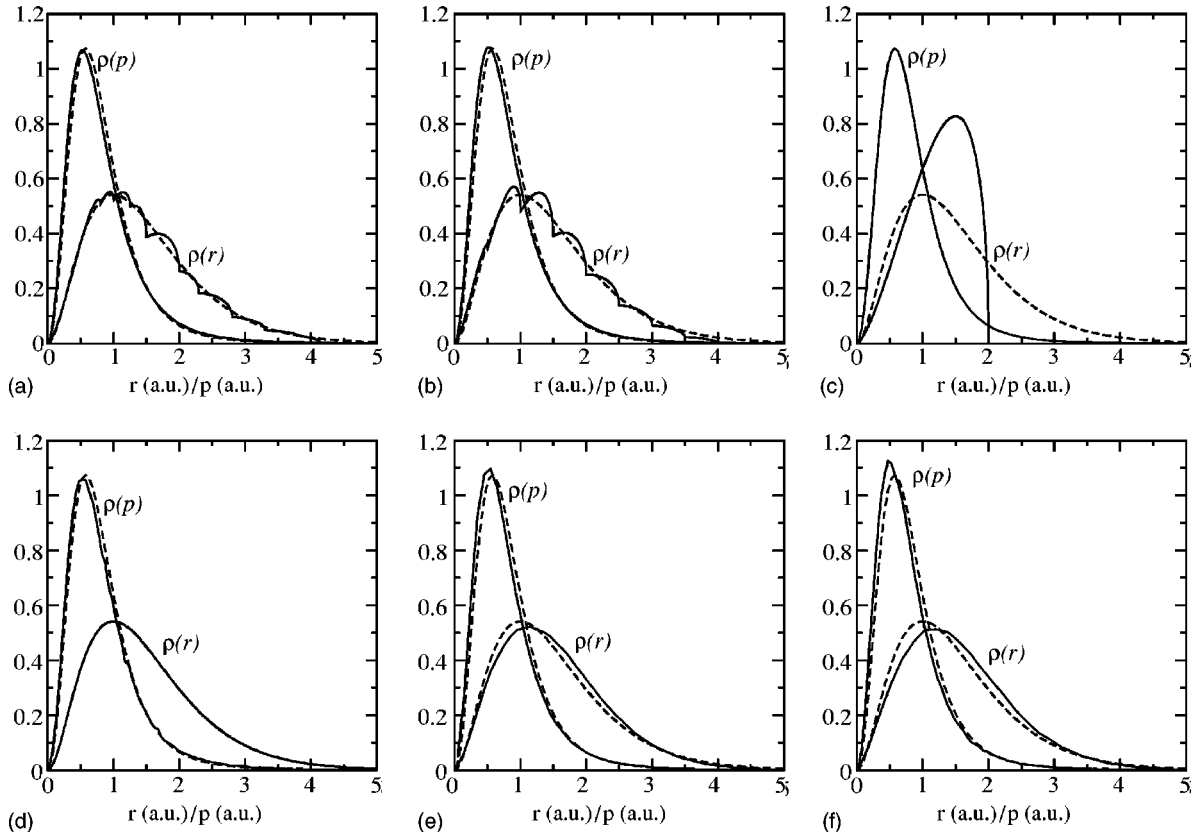

FIG. 2. Spatial and momentum initial densities as functions of r (in a.u.) and p (in a.u.), respectively, for H(1s): - - -, quantum. (a) —, ten microcanonicals. (b) —, eight microcanonicals. (c) —, single microcanonical. (d) —, Cohen (see Table II) (spatial density is identical to quantum one). (e) —, Gaussian (see Table II). (f) —, Raković *et al.* (see Table II).

there is an overall improvement of the accuracy when Eq. (6) or (7) is used as initial distribution rather than the single-microcanonical choice, especially at low velocities. This can be reasoned to be due to the fact that the ionization process mainly involves the outer part of the 1s electron cloud, and is consequently inhibited when one uses a description for this cloud that is too compact. Incidentally, we note that our single-microcanonical data agree well with those of Olson and Salop [6], who used a rather limited number of trajectories: this indicates that statistically converged impact-parameter and three-body CTMC cross sections are identical, as can be expected from the success of the impact-parameter approximation in the semiclassical context [13].

Turning now to the finer comparison between the CTMC results using different initial conditions of the type of Eq. (6)

TABLE I. Coefficients w_i, energies E_i, average energy $\langle E\rangle$, and standard deviation S for the sum of eight and ten microcanonical ensembles

	Eight microcanonicals		Ten microcanonicals	
i	$-E_i$	w_i	$-E_i$	w_i
1	2.0	0.016	1.25	0.030
2	1.0	0.098	1.0	0.045
3	0.66	0.1923	0.8	0.069
4	0.5	0.2185	0.66	0.150
5	0.4	0.1849	0.5	0.187
6	0.33	0.1349	0.435	0.135
7	0.28	0.092	0.36	0.156
8	0.25	0.063	0.3	0.099
9			0.26	0.032
10			0.24	0.092
$\langle E\rangle$	−0.528		−0.509	
S	0.047		0.031	

TABLE II. Forms of energy density functions $\rho_E(E)$. The average energy is for [34] $\langle E\rangle=-0.5$; [33], $\langle E\rangle=-0.478$; Gaussian, $\langle E\rangle=-0.5$. $E=-1/2n_c^2$.

	ρ_E
[34]	$\frac{\sqrt{\pi}}{4\lvert E\rvert^4}e^{1/E}\left[\frac{1}{4}W_{-1/2,-1/2}\left(-\frac{2}{E}\right)-\left(1+\frac{2}{E}\right)W_{1/2,-1/2}\left(-\frac{2}{E}\right)\right]$ [a]
[33]	$\frac{\sqrt{2}\pi^3}{25.66}n_c^5e^{-10.1(n_c-1)^2}$
Gaussian	$2.75e^{-11.95(n_c-1.2)^2}$

[a] $W_{\kappa,\mu}(z)$ stands for Whittaker's function (see [54]).

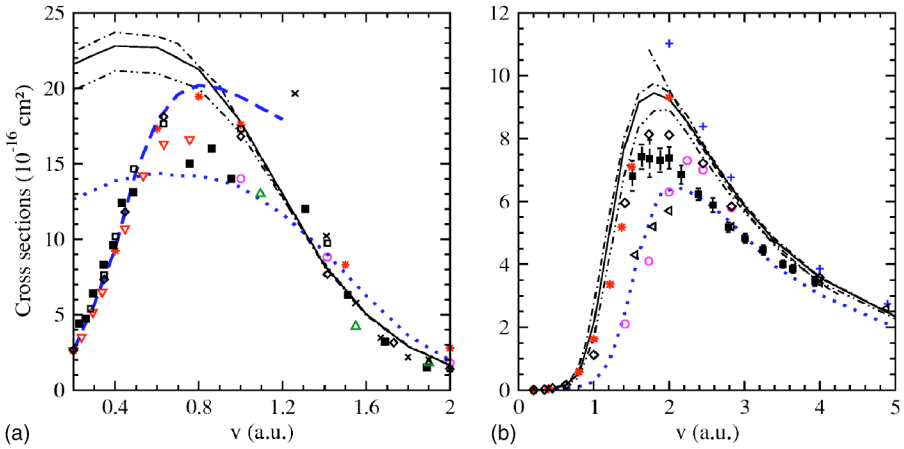

FIG. 3. Capture (a) and ionization (b) cross sections as functions of the relative nuclear velocity v for $Li^{3+}+H(1s)$ collisions:—, present OEDM (88 states) molecular results; ∗, OEDM+GTO. Present classical results for different initial distributions (see Table II): ⋯, single microcanonical; - · -, Cohen; - ·· -, sum of eight microcanonical distributions; —, sum of ten microcanonical distributions. Other theoretical results: ○, [5]; ▽, [38]; △, [44]; ×, [42]; □, [39]; ◇, [43]; ◁, [40]; +, [55]; - - · - -, [45]. Experimental results: ●, [36]; ■, [35,37].

or (7), we see that, although there is a slight improvement of our fit with ten microcanonical distributions over the previous one of Hardie and Olson [15], discrepancies between the use of different choices in Eq. (7) are very small. Similarly, the results using in Eq. (6) the distribution of Cohen [34], Raković *et al.* [33], and our Gaussian form (Table II) are so close to each other that in Fig. 3 and in the following we shall quote only the Cohen result. In addition, discrete (7) and continuous (6) superpositions also yield close results. For the sake of conciseness, we do not illustrate the fact that all these agreements also hold for the partial cross sections.

Our calculated capture and ionization cross sections for the $Ne^{10+}+H$ system are displayed in Fig. 4, where we have included other theoretical [5,46–51] and experimental [52] results. Again, comparison of these data with our calculations is analyzed in Paper I. The total capture probabilities [Eq. (14)] are given in Fig. 5 for some selected v values. We shall only emphasize the accuracy of the close-coupling data, which are as good as for the previous system. We see from Fig. 4 that the cross sections obtained with the CTMC and close-coupling methods agree with each other much better than in the previous case, and for the whole domain considered (down to $v=0.2$ a.u.). In fact, the reader may wonder why we did not consider smaller nuclear velocities to find out the "domain of validity" of the method for highly charged projectiles; the reason will be apparent in the next section. We also see from the figure that a sizable improvement follows by using the initial conditions of Eqs. (6) and (7) rather than the single-microcanonical choice, for both capture and ionization. Discrepancies between the use of different initial densities in Eqs. (6) and (7) are slightly larger than before, but are still very small, and are of the same order as the small divergence with respect to the semiclassical data. Use of the ten-microcanonical fit appears to fare best.

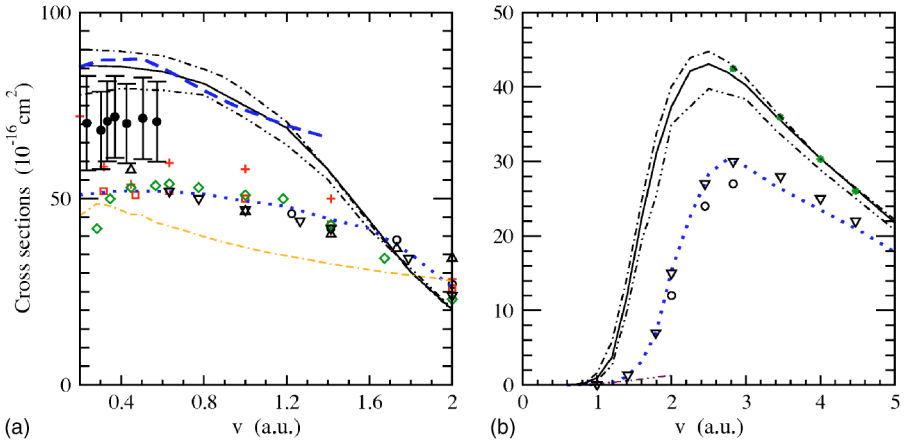

FIG. 4. Total capture (a) and ionization (b) cross sections in $Ne^{10+}+H(1s)$ collisions, as functions of the relative nuclear velocity v:—, present OEDM (213 states) molecular results; ∗, spherical Bessel monocentric expansion. Present classical results for different initial distributions: ⋯, single microcanonical; - · -, Cohen; - ·· -, sum of eight microcanonical distributions; —, sum of ten microcanonical distributions. Other CTMC calculations: △, [47]; ○, [5]; □, [48]; ▽, [49]·—·—, Hidden crossing calculations[46]. Perturbative calculations: +, [50]; ◇, unitarized distorted wave approximation (UDWA) [51]. Experimental results: ●, [52].

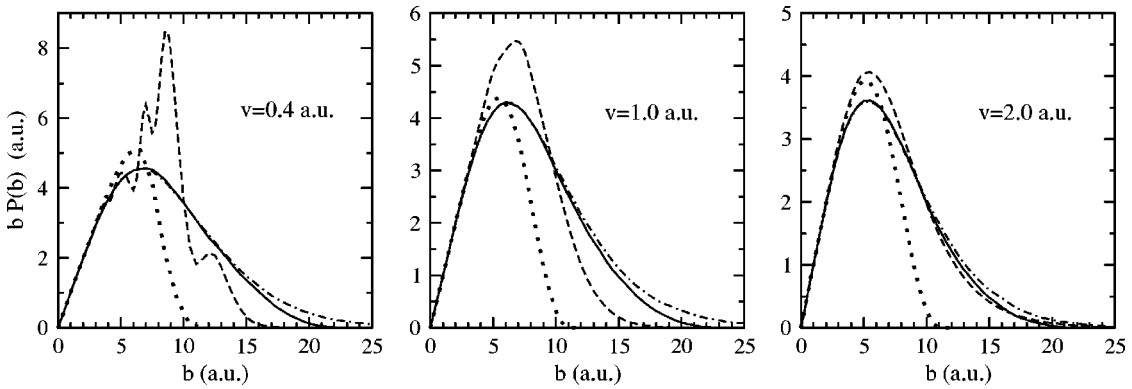

FIG. 5. Capture probabilities $P(b)$ times the impact parameter b, as functions of b (in a.u.), for $Ne^{10+}+H(1s)$ collisions at different impact velocities (for $v=2$ a.u. results correspond to e-loss probabilities): - - -, OEDM; —, 10 microcanonicals; - · -, Cohen; ···, single microcanonical.

The previous encouraging features are tempered by the finding, reported in Paper I, that the low-v agreement between CTMC and close-coupling total capture cross sections is less good for the partial ones. Hence, the domain of validity of the method can be stated to be similar for Li^{3+} and for Ne^{10+} projectiles. This feature of accurate total cross sections and poorer partial ones can only be the result of a cancellation of errors, and we found that this is indeed the case. Moreover, the compensation depends little on the initial distribution, although the use of the superposition of eight or ten microcanonical distributions [Eq. (7) and Table I] appears to behave better than the continuum ones [Eq. (6) and Table II]. The compensation effect does not take place for the partial cross sections, and at higher velocities ($v>2$ a.u.), the classical probabilities become accurate. To examine some of the reasons why the method fails at low v, we now study the mechanisms.

VI. COMPARISON OF MECHANISMS

The first question of a comparative study of the dynamics described by the CTMC and semiclassical methods is whether they describe a common mechanism. Such is the case of ionization, for which it was shown in Ref. [14] that even the time-dependent spatial and momentum densities are alike. It is not easy, however, to extend that analysis to electron capture, where the main difficulty is to choose what should be compared, or contrasted. For instance, drawings of the overall densities yield similar pictures which are not illustrative enough because of their compact structure. On the other hand, the usual way to analyze mechanisms using the molecular approach makes use of the so-called "collision history", given by the evolution of the populations [the modulus squared of the expansion coefficients, $|a_n(t)|^2$; see Eq. (3)] of the molecular channels along selected nuclear trajectories. A more compact, related quantity is the electronic molecular energy, which is the expectation value of the clamped-nuclei Hamiltonian:

$$E_{\mathrm{mol}}^{cc}(t)=\sum_n |a_n(t)|^2 E_n(R(t)). \tag{17}$$

This quantity depends on both the individual probabilities and energies, differing when the total probabilities coincide but the partial ones do not. To obtain the CTMC counterpart, we must first define electronic velocities with respect to fixed nuclei. This is readily done by substracting from the electronic momenta $\mathbf{p}$ the drag from the nuclear motion $f(\mathbf{r},\mathbf{R})\mathbf{v}$, in an inverse procedure to the introduction of common ETFs in close-coupling calculations [16,53], with the same switching function $f(\mathbf{r},\mathbf{R})$ [see Eq. (4)] employed in the close-coupling calculation [21]. The molecular energy of the discretized classical electrons distribution then reads:

$$E_{\mathrm{mol}}^{\mathrm{CTMC}}(t)=\frac{1}{N}\sum_{i=1}^{N}\left\{\frac{1}{2}[\mathbf{p}_i-f(\mathbf{r}_i,\mathbf{R})\cdot\mathbf{v}]^2-\frac{1}{r_i}-\frac{Z_p}{|\mathbf{r}_i-\mathbf{R}|}\right\}. \tag{18}$$

In the quantal molecular approach, electron transfer mostly takes place through transitions between the molecular states in the pseudocrossing regions of the correlation diagram. In the classical approach, one substitutes this mechanism involving dicrete states by one involving continua (or quasicontinua), with a collisional energy density $\rho_{\mathrm{mol}}(E_{\mathrm{mol}})$, with mean value $E_{\mathrm{mol}}^{\mathrm{CTMC}}(t)$ and statistical dispersion

$$s(t)=\sqrt{\frac{1}{N}\sum_{i=1}^{N}\left\{\frac{1}{2}[\mathbf{p}_i-f(\mathbf{r}_i,\mathbf{R})\cdot\mathbf{v}]^2-\frac{1}{r_i}-\frac{Z_p}{|\mathbf{r}_i-\mathbf{R}|}-E_{\mathrm{mol}}^{\mathrm{CTMC}}\right\}^2}. \tag{19}$$

One can then expect that the more quantal molecular energies are included in a unit energy interval, the more accurate can the classical approach be expected to be. In practice, therefore, one may expect more problems at low velocities, where the behavior of the collisional wave function at the critical inner pseudocrossing becomes adiabatic, and the cross section falls.

We can study this point and follow the workings of $\rho_{\rm mol}(E_{\rm mol})$ in the classical mechanism by considering the evolution, for a given nuclear trajectory, of the collisional energy band $[E_{\rm mol}^{\rm CTMC}-\sqrt{2}\varsigma, E_{\rm mol}^{\rm CTMC}+\sqrt{2}\varsigma]$ about $E_{\rm mol}^{\rm CTMC}$. Obviously, for a single-microcanonical distribution ς is initially zero, and increases at small distances where electron capture take place, whereas for the hydrogenic initial state it is initially given by the dispersion of the distributions in Eqs. (6) and (7), and accordingly its final value is larger than the single-microcanonical one. For a given impact parameter, one can then qualitatively gauge the size of the transition probability to a given n level by a consideration of the overlap of the energy band with that of an empirical molecular bin. This can be obtained from an extrapolation to the molecular states of the binning method for the projectile states, given by

$$E_{\rm mol}^{n}(R)=\left[\frac{1}{(n+1)^2}-\frac{1}{n^2}\right]^{-1}\left\{\left[\frac{1}{c^{(n)2}}-\frac{1}{n^2}\right]E_{n+1}(R)+\left[\frac{1}{(n+1)^2}-\frac{1}{c^{(n)2}}\right]E_n(R)\right\}, \tag{20}$$

which has the property that it tends to the atomic value at infinite nuclear separations:

$$E_{\rm mol}^{n}(R)\rightarrow_{R\rightarrow\infty}E^{(n)}, \tag{21}$$

with $E_n(R)$ and $E_{n+1}(R)$ the molecular quantal energies of Eq. (17) and $c^{(n)}$ and $E^{(n)}$ defining the corresponding atomic bins as given in Sec. III. One may then reason that the larger the overlap and the larger $\rho_{\rm mol}(E_{\rm mol})$ in the overlap region (e.g., the smaller the corresponding width ς there), the larger the transition probability. We have checked the overall applicability of this rule of thumb; we shall present some illustrations, and quote other results.

In our analysis of the mechanisms, we have further split the energies (17) and (18) into kinetic and potential parts; we have studied individual electron trajectories in the classical case, and the collision histories in the semiclassical calculations; and we have drawn the time variation of the quantal [$\mathbf{j}_Q$ of Eq. (2)] and classical [$\mathbf{j}$ of Eq. (5)] current density, obtained, as in Ref. [14], by a local averaging process. Although we have also studied the case of $Li^{3+}+H$, we restrict our illustrations to the more "problematic" case of Ne^{10+} projectiles. We consider in Figs. 6(a)–6(c) the relative velocity $v=1$ a.u., and three impact parameters: $b=10$ [Fig. 6(a)], 7 [Fig. 6(b)], and 3 a.u. [Fig. 6(c)]. It is useful to examine these figures together with the drawings of the transition probabilities to $n=4$ [Fig. 7(a)], 6 [Fig. 7(b)], and 8 [Fig. 7(c)], as functions of the impact parameter b.

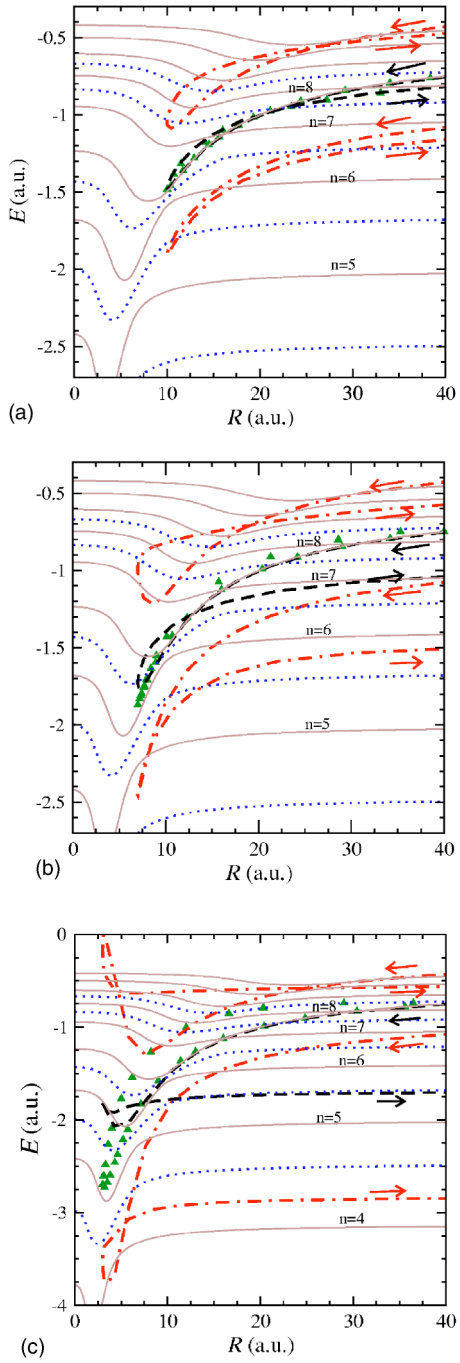

FIG. 6. Energy correlation diagram for the NeH^{10+} quasimolecule. For $v=1$ a.u. and three impact parameters b (a) 10, (b) 7, (c) 3 a.u. we also give the energy curves for the classical mean molecular energy $E_{\rm mol}^{\rm CTMC}$ (- - -) and the values for $E_{\rm mol}^{\rm CTMC}\pm\sqrt{2}\varsigma$ (- . -), yielding a dynamical energy band. This is to be compared with the exit bands obtained from an empirical molecular binning proceeding, defined by the values of $E_{\rm mol}^{n}$ [Eq. (20)] (···). Close-coupling electronic molecular energy $E_{\rm mol}^{\rm cc}$ is also represented by (▲).

Figure 6(a) shows that both $E_{\rm mol}^{\rm cc}$ and $E_{\rm mol}^{\rm CTMC}$ diabatically follow the energy of the entrance channel $E_{10\ 9\ 0}$ (with parabolic quantum numbers 10 9 0) in the way in to the collision: this means for instance that at $R=40$ a.u. it becomes E_{980}; at

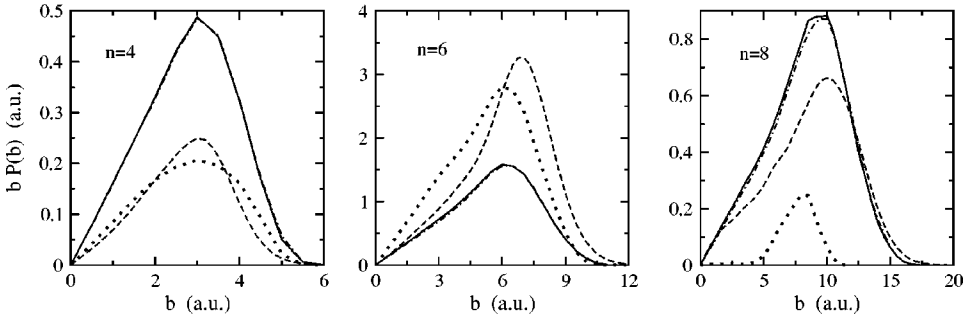

FIG. 7. State-selective transition probabilities $bP(b)$ as functions of b (in a.u.), for a $Ne^{10+}+H(1s)$ collision at impact velocity $v=1.0$ a.u.: - - -, OEDM; —, ten microcanonicals; - · -, Cohen; ···, single microcanonical.

$R=25$ a.u., E_{870}; and so on. In the way out from the collision ($t>0$), the values of the molecular energies are given by roughly the same combination of this initial energy and E_{760} and E_{650} so that $E_{\mathrm{mol}}^{\mathrm{cc}} \approx E_{\mathrm{mol}}^{\mathrm{CTMC}}$. The physical mechanism as given by the variation of the current density vector diagrams consists in a part of the electron cloud being attracted by the projectile and captured by it; the captured cloud first rotates about the projectile, and finally shares its velocity along the Z axis. We can now employ the overlap criteria between collisional and BM energy bands, described above, to explain why transitions to the high-lying energy levels are reasonably well reproduced by the CTMC calculations [Fig. 7(c)], since the corresponding partial cross sections are dominated by the contributions of large impact parameters. Incidentally, we mention that the corresponding overlaps with the single-microcanonical results are extremely small, thereby explaining why this method is unsuitable to treat transitions to those states—just as it cannot describe ionization at threshold.

Similarly, the energies $E_{\mathrm{mol}}^{\mathrm{cc}}$ and $E_{\mathrm{mol}}^{\mathrm{CTMC}}$ in Fig. 6(b) have roughly the same behavior. In this case, the electron cloud strongly accelerates as it approaches the projectile, and this results in a sudden increase of the electronic kinetic energy when the two nuclei are closest, giving rise to the peculiar "loop" of the molecular energies in the figure. We find, however, a limitation of the method that can be ascribed to an inadequacy of the lower limit of the collisional band. This appears to be a little too low so that $\rho_{\mathrm{mol}}(E_{\mathrm{mol}})$ is too diffuse there, so that the probabilities to $n=5$ and 6 [see Fig. 7(b)] are underestimated. In turn, this behavior of the collisional band can be attributed to a value for the smallest energy in Eq. (7) (a rather arbitrary quantity) that is too low. Thus, the results of using a single-microcanonical distribution are better, because then one finds that the lower limit of the collisional band lies slightly higher up.

These features are considerably enhanced in Fig. 6(c) for $b=3$ a.u., in which case the collisional band even penetrates too much in the $n=4$ BM band, with the results that probabilities to $n=4$ are considerably overestimated [Fig. 7(a)], and the limitations of the method stand out clearly.

In addition to the previous features, we find that the classical method cannot, as expected, reproduce the destructive interference of the phases in the amplitudes of the molecular states (mainly the 760 and 650 states) in the way out of the collision. At lower velocities, this well-known interference phenomenon gives rise to noticeable Stückelberg oscillations in the probability, which are visible in Fig. 5. Finally, at even lower impact parameters (not illustrated here), the molecular energies display a double "loop," due to the rotation of the electron cloud (first loop), in which the electrons are so much accelerated that they issue with a velocity that is about $2v$; later on in the way out of the collision, the drag from the projectile reduces this speed to v (second loop). In this case, when considering spatial densities, one has the curious optical effect that the accelerated cloud appears to be pushed by the projectile rather than being captured by it. It is noteworthy that in this way out of the collision, the quantal description of the electron cloud follows the same mechanism through a complicated set of transitions to bonding molecular orbitals (quantum numbers 760, 650, 540, 430) at first, and then to antibonding ones (quantum numbers 700, 710, 610, 600, 500, 400) in order to describe the accelerated cloud traveling in front of the projectile.

VII. CONCLUSIONS

This work reports our findings on the accuracy of CTMC treatments of electron capture in atomic collisions, which were obtained in the course of the work reported in Paper I; for this purpose, we have extended our calculations to such low velocities that the limitations of the classical method are highlighted. In our analysis of these limitations, we have taken up a pragmatic viewpoint, in view of the difficulty of setting up a suitable working scheme to relate classical and quantal (or semiclassical) approaches: although either the WKB or the Moyal-Wigner method would formally appear to provide such a formal scheme, since they tend to the classical approach in the $\hbar \to 0$ limit, we have argued that neither of them is really appropiate. Thus, while the WKB method has been widely used for nuclear trajectories, and has the asset of providing a hierarchy of approximations from the purely classical to the purely quantal formalism, it yields a grossly inaccurate classical description of the initial state of the collisional system, unlike the CTMC method. On the other hand, the statistical Moyal-Wigner approach is unwieldy, and is unsuitable to provide suitable classical initial states or the corrections to the Hamilton equations employed in the CTMC treatment.

Because of this difficulty, we have chosen to focus on the accuracy of specific capture and ionization probabilities and cross sections. As in Paper I, we have focused on collisions on H(1s) targets, and low-charged (Li^{3+}) and high-charged (Ne^{10+}) projectiles. For Li^{3+}, there is a wealth of accurate theoretical and experimental data, and we have added to these data our results of close-coupling calculations employing a very large molecular basis including pseudostates. We

have then extended our study to Ne^{10+} projectiles, for which there is little information, and which has recently become of interest in fusion work. As a result of our encouraging findings, a systematic calculation of capture and ionization cross sections for other systems such as $Ar^{q+}+H$, which is very difficult to treat with close-coupling methods, is presently under way.

In practice, a CTMC calculation involves three main steps, to wit, constructing the initial probability distribution, carrying out the classical trajectory calculations, and obtaining the probabilities. While the second step is basically standard, the other ones involve what are, to some extent, optional ways of imposing "quantal" conditions in an otherwise classical formulation. We have thus investigated whether using different proposed initial conditions changes the results, and whether the usual BM partitioning method for the exit states is appropriate. With respect to the former, we find that substituting the single-microcanonical description of the initial state by a sum [Eq. (4)] or integral [Eq. (3)] over microcanonical distributions significantly improves the results for the ionization and total electron capture cross section. On the other hand, those results are quite insensitive to the fine details of the improved initial state. This is good news for the users of the method, but it also means that when the method fails, little improvement can be reached in general by making the description of the initial state of the system more sophisticated.

With respect to the final states, we have illustrated how the binning procedure yields a reasonable description of the outer part of the electronic densities of atomic states with $n>2$, the better for larger angular momentum, which is quite reasonable from the way the method was developed. Unfortunately, the procedure is useless to describe the $H(1s)$ initial state, and the separation between the subsets corresponding to $H(1s)$ and $H(n=2)$ is rather artificial. This means that cross sections to Li^{2+} and $Ne^{9+}(n=1)$, of no importance in the present context, cannot be expected to be accurate. More importantly, this would also affect excitation to $H(n=2)$, which was not treated here. Because of this limitation, the CTMC method as is usually employed is limited to not-too-low principal quantum numbers.

For higher-lying states, our main conclusion regarding the overall accuracy of the CTMC method is quite encouraging, and many of the previous findings on its accuracy for ionization extend to electron capture for high n numbers. In fact, at intermediate energies, CTMC and atomic close-coupling results for the total cross sections agree with each other, and are probably more accurate than experiment with regard to both ionization and capture. We have reasoned that the basis for such a success for electron transfer must be similar as for ionization, and must rely on a dominance of two-body interactions in the capture process. A good proof that this is so is that CTMC and semiclassical methods essentially describe the same mechanism, as mentioned in the previous section. On the other hand, at low velocities, the situation is not so good as could be deemed from the cross sections: for Ne^{10+} projectiles, we have also seen that the accuracy of the total charge exchange cross section does not quite extend to the partial ones, and in particular, the partial cross sections to $n=4$ are overestimated, while those to $n=5$, 6 are underestimated. Consideration of the mechanisms involved has enabled us to trace this limitation to the fact that the superpositions (6) or (7) that are employed to represent the initial distribution involve unphysically low energies. There seems to be no way round this problem as long as one employs the spatial and momentum distributions to gauge the quality of this distribution, and requires the mean initial energy to be about -0.5 hartree. Use of a single-microcanonical distribution is free from this liability, but then transitions to high-lying and ionizing states are worse represented. Finally, the problem takes place in a velocity domain where interference effects also start to take place in the physical (quantal) mechanism.

ACKNOWLEDGMENTS

This work has been partially supported by DGICYT Projects No. BFM2000-0025 and No. FTN2000-0911. We would like to acknowledge the Ministerio de Ciencia y Tecnología (Spain) and the Ministère des Affaires Etrangères (France) for financial support under the coordinated program AIHF04-Picasso2004. C.I. would also like to acknowledge the UAM for support under a research contract.

[1] R. Abrines and I. C. Percival, Proc. Phys. Soc. London **88**, 861 (1966).
[2] I. C. Percival and D. Richards, Adv. At. Mol. Phys. **11**, 1 (1973).
[3] C. O. Reinhold and C. A. Falcón, J. Phys. B **21**, 1829 (1988).
[4] C. O. Reinhold and J. Burgdorfer, J. Phys. B **26**, 3101 (1993).
[5] R. Olson and A. Salop, Phys. Rev. A **16**, 531 (1977).
[6] R. Olson and A. Salop, Phys. Rev. A **16**, 1811 (1977).
[7] R. Olson, Phys. Rev. A **24**, 1726 (1981).
[8] C. Illescas and A. Riera, Phys. Rev. A **60**, 4546 (1999).
[9] K. B. MacAdam and E. Horsdal-Pedersen, J. Phys. B **36**, R167 (2003).
[10] J. Pascale, R. E. Olson, and C. Reinhold, Phys. Rev. A **42**, 5305 (1990).
[11] A. R. Schlatmann, R. Hoekstra, R. Morgenstern, R. E. Olson, and J. Pascale, Phys. Rev. Lett. **71**, 513 (1993).
[12] H. O. F. L. Meng, R. E. Olson, and R. Hoekstra, J. Phys. B **27**, 2269 (1994).
[13] B. H. Bransden and M. H. C. McDowell, *Charge Exchange and the Theory of Ion-Atom Collisions* (Clarendon, Oxford, 1992).
[14] C. Illescas, B. Pons, and A. Riera, Phys. Rev. A **63**, 062722 (2001).
[15] D. J. W. Hardie and R. E. Olson, J. Phys. B **16**, 1983 (1983).
[16] C. Illescas, I. Rabadan, and A. Riera, Phys. Rev. A **57**, 1809 (1998).

[17] C. Illescas and A. Riera, Phys. Rev. Lett. **80**, 3029 (1998).
[18] C. Illescas, B. Pons, and A. Riera, Phys. Rev. A **65**, 030703(R) (2002).
[19] L. F. Errea, C. Harel, H. Jouin, L. Méndez, B. Pons, A. Riera, and I. Sevila, Phys. Rev. A **65**, 022711 (2002).
[20] L. F. Errea, L. Méndez, B. Pons, A. Riera, and I. Sevila, Phys. Rev. A **67**, 022716 (2003).
[21] L. F. Errea, C. Illescas, L. Méndez, B. Pons, A. Riera, and J. Suárez, J. Phys. B **37**, 4323 (2004).
[22] S. B. Schneiderman and A. Russek, Phys. Rev. **181**, 311 (1969).
[23] L. F. Errea, C. Harel, H. Jouin, L. Méndez, B. Pons, and A. Riera, J. Phys. B **27**, 3603 (1994).
[24] C. Harel and H. Jouin, Europhys. Lett. **11**, 2121 (1990).
[25] C. Harel and H. Jouin, J. Phys. B **24**, 3219 (1990).
[26] J. S. Burlisch and J. Stoer, Numer. Math. **8**, 1 (1966).
[27] R. L. Becker and A. D. MacKellar, J. Phys. B **17**, 3923 (1984).
[28] E. P. Wigner, Phys. Rev. **40**, 749 (1932).
[29] J. E. Moyal, Proc. Cambridge Philos. Soc. **45**, 99 (1949).
[30] N. G. D. Eichenauer and W. Scheid, J. Phys. B **14**, 3929 (1981).
[31] R. G. P. I. Samego and R. O. Barrachina, J. Phys. B **32**, 1971 (1999).
[32] A. Salop, J. Phys. B **12**, 919 (1979).
[33] M. J. Raković, D. R. Schultz, P. C. Stancil, and R. K. Janev, J. Phys. A **34**, 4753 (2001).
[34] J. S. Cohen, J. Phys. B **18**, 1759 (1985).
[35] M. B. Shah and H. B. Gilbody, J. Phys. B **11**, 121 (1978).
[36] W. Seim, A. Müller, I. Wirkner-Bott, and E. Salzborn, J. Phys. B **14**, 3475 (1981).
[37] M. B. Shah and H. B. Gilbody, J. Phys. B **15**, 413 (1982).
[38] W. Fritsch and C. D. Lin, J. Phys. B **15**, 1255 (1982).
[39] H. J. Lüdde and R. M. Dreizler, J. Phys. B **15**, 2713 (1982).
[40] D. S. F. Crothers and J. F. McCann, J. Phys. B **16**, 3229 (1983).
[41] M. B. Shah and H. B. Gilbody, J. Phys. B **18**, 899 (1985).
[42] D. Belkič, R. Gayet, and A. Salin, At. Data Nucl. Data Tables **51**, 76 (1992).
[43] N. Toshima, Phys. Rev. A **50**, 3940 (1994).
[44] M. S. Gravielle and J. E. Miraglia, Phys. Rev. A **51**, 2131 (1995).
[45] F. Martín, J. Phys. B **32**, 501 (1999).
[46] D. R. Schultz and P. S. Krstic, At. Plasma-Mater. Interact. Data Fusion **6**, 173 (1996).
[47] T. P. Grozdanov, J. Phys. B **13**, 3835 (1980).
[48] J. A. Perez, R. E. Olson, and P. Beiersdofer, J. Phys. B **34**, 3063 (2001).
[49] G. Maynard, R. K. Janev, and K. Katsonis, J. Phys. B **25**, 437 (1992).
[50] H. Ryufuku and T. Watanabe, Phys. Rev. A **20**, 1828 (1979).
[51] N. Toshima and T. Watanabe, Phys. Rev. A **33**, 1382 (1986).
[52] F. W. Meyer, A. M. Howald, C. C. Havener, and R. A. Phaneuf, Phys. Rev. A **32**, 3310 (1985).
[53] G. Bandarage and R. Parson, Phys. Rev. A **41**, 5878 (1990).
[54] *Handbook of Mathematical Functions*, edited by M. Abramowitz and I. A. Stegun (Dover, New York, 1965).
[55] I. Sevila, Ph.D. thesis, Universidad Autónoma de Madrid, 2003.